Eccentricity matters: Impact of eccentricity on inferred binary black hole populations

M. Zeeshan[*] and R. O'Shaughnessy[†]

Center for Computational Relativity and Gravitation, Rochester Institute of Technology, Rochester, New York 14623, USA

(Received 2 May 2024; accepted 12 August 2024; published 5 September 2024)

Gravitational waves (GWs) emanating from binary black holes (BBHs) encode vital information about their sources, enabling us to infer critical properties of the BBH population across the Universe, including mass, spin, and eccentricity distribution. While the masses and spins of binary components are already recognized for their insights into formation, eccentricity stands out as a distinct and quantifiable indicator of formation and evolution. However, despite its significance, eccentricity is notably absent from most parameter estimation analyses associated with GW signals. To evaluate the precision with which the eccentricity distribution can be deduced, we generated two synthetic populations of eccentric binary black holes (EBBHs) characterized by nonspinning, nonprecessing dynamics, and mass ranges between 10 and $50M_{\odot}$. This was achieved using an eccentric power law model, encompassing 100 events with eccentricity distributions set at $\sigma_\epsilon = 0.05$ and $\sigma_\epsilon = 0.15$. This synthetic EBBH ensemble contrasts against a circular binary black holes collection to discern how parameter inferences would vary without eccentricity. Employing Markov chain Monte Carlo techniques, we constrained model parameters, including the event rate ($\mathcal{R}$), minimum mass ($m_{\rm min}$), maximum mass ($m_{\rm max}$), and σ_ϵ which is uncertainty in eccentricity. Our analysis demonstrates that eccentric population inference can identify the signatures of even modest eccentricity distribution. In addition, our study shows that an analysis neglecting eccentricity may draw biased conclusions of population inference for the larger values of eccentricity distribution.

DOI: 10.1103/PhysRevD.110.063009

I. INTRODUCTION

Black holes exist in different sizes and types [1]. When two black holes become gravitationally bound, they form a binary and start coalescing [2]. When they coalesce, they produce ripples in the fabric of space-time, known as GW [1]. These waves are the primary way to detect those mergers in space, starting with LIGO's [3] first detection of a BBH merger (GW150914). Afterward, the LIGO-VIRGO-KAGRA (LVK)network [3–6] continued to regularly detect gravitational waves from various compact binaries such as BBH, binary neutron stars (BNSs), and binaries composed of a neutron star and black hole (NSBH) [7–10]. These waves carry information about the progenitor, such as component mass, spin, period, eccentricity, distance, and location. Indirectly, these properties may provide clues into how binaries are formed. These binaries are believed to form from isolated and dynamic formation scenarios [11]. The isolated binaries are thought to result from the death of binary stars, either by a supernova or a common envelope [12,13]. On the other hand, two black holes can also make a binary through dynamic encounters in dense star clusters [14,15]. Importantly, each formation scenario imprints on binary parameters such as mass, spin, and eccentricity. For instance, isolated binaries tend to have circular orbits in the LVK band due to mass transfer and most probably the result of gravitational decay over time. On the contrary [12], the dynamically formed binaries may have eccentric orbits.

Mass and spin are widely used to understand a binary's properties, evolution, and formation channel. However, many of these same formation scenarios can also introduce eccentricity in BBH orbits, such as stellar scattering, dynamic interactions in dense environments, or interaction of a third object with a binary. Furthermore, low energy and slow-forming binaries usually start with modest eccentricities but at very low frequencies, and over many decades of frequency evolution, gravitational wave radiation circularizes their orbits [16] before entering the LVK frequency band. However, binaries formed in more violent, energetic environments, such as globular clusters, can be formed closer to the LVK frequency band and thus retain more of their large natal eccentricities when observationally accessible. Previous studies have demonstrated that identifying orbital eccentricity could differentiate between formation channels [17–21].

[*]Contact author: m.zeeshan5885@gmail.com
[†]Contact author: richardoshaughnessy.rossma@gmail.com

Although eccentricity is a signature that can be measured with GW and is unique to extreme events such as high mass ratio mergers, all the confirmed detections so far may be consistent with a nearly circular orbit in the LVK frequency band [22,23]. However, some investigations suggest that BBHs like GW190521 may exhibit some indications of eccentricity [24–28]. On the other hand, we have studies [29,30] which do not find evidence of eccentricity in GW190521. So, whether eccentricity is present in the GW190521 or not is still an exciting event. Unfortunately, these inferences rely on incompletely surveyed waveforms produced by direct simulation or (more customarily) by phenomenological approximations tuned to those simulations. Currently, available phenomenological models allowing for eccentricity only cover part of the possible parameters: nonprecessing binaries, for example. While researchers are actively producing the eccentric waveform models analytically [31] and numerically [32–36], at present, parameter inference capabilities are limited.

Despite severe limitations on single-event parameter inference, a few proof-of-concept studies have investigated how to identify the presence of an eccentric subpopulation from observations of many massive binary black holes [37–39]. The techniques used in these investigations borrow from extensive studies on reconstructing the population properties of quasicircular binaries over the whole mass spectrum [40–50]. Because eccentricity is poorly constrained by short GW observations of massive BH binaries, these studies find eccentricity can only be resolved with great difficulty, even with many observations.

By contrast, previous studies have demonstrated that eccentricities can be particularly well constrained for low-mass objects [51], owing to their long modulated inspiral [52], even it improves the accuracy in parameter inference [53]. We use this parameter inference investigation as our prototype for the inferences about synthetic GW sources in our proof-of-concept study.

In this study, we focused on the nonspinning, nonprecessing, lower mass $(10-50M_\odot)$. In addition, we will use mass ratio $q = m_1/m_2$ with condition $m_1 > m_2$ and total mass $M = m_1 + m_2 = 100M_\odot$. We also infer how well we can recover the event rate, mass, and eccentricity distribution using the 100 eccentric events. To extend our analysis, we compared constrained parameters using the eccentric binary black holes (EBBHs) and circular binary black holes (CBBHs), which show a considerable difference in the recovery of true parameter for higher eccentric ($\sigma_\epsilon = 0.15$) population and similar recovery for lower eccentric population ($\sigma_\epsilon = 0.05$), here σ_ϵ is the uncertainty in eccentricity.

In Sec. II, we described the Bayesian statistical methods used to make the population inference. Briefly, we also described the volume-time estimate to accommodate the LVK sensitivity. We modified the previously constructed [54,55] power law model to include eccentricity using a truncated normal distribution. We used this model to generate a synthetic population and then made the inference using the Markov chain Monte Carlo (MCMC) method. Section III describes how we have created a synthetic population using the eccentric power law model and then added an error in each event to make the population closer to real events detectable by LVK. Second, we explained the scaling to remove the eccentricity from the synthetic events to compare the different constraints using EBBH and CBBH populations. Section IV explains how well we can constrain the population parameters using EBBH vs CBBH. Section V discusses the importance of eccentric binaries, and finally, we conclude our findings in Sec. VI.

II. METHODS

A coalescing BBH can be entirely described by three intrinsic and seven extrinsic parameters. The intrinsic parameters, such as the mass of the binary component (m_i), spin (χ_i), and eccentricity (ϵ), determine the orbital evolution of the binary. The extrinsic parameters determine the merger's space-time coordinates and orientation. We used the following method to infer the population properties of binary black holes.

A. Hierarchical Bayesian modeling

We use hierarchical Bayesian modeling (HBM) to constrain a population model with gravitational wave data. In HBM, we have N number of discrete detections. Those detections provide merger data denoted as $d_1, d_2, d_3, \ldots, d_N$, where each d_i shows a BBH merger. Each stretch of data d_i can be used to infer the properties of the BBH associated with that data segment. These properties, often called parameters, are denoted by $\lambda_1, \lambda_2, \lambda_3, \ldots, \lambda_i$. Each parameter has its uncertainty, and we express it by the probability of the data given the parameter value. We also refer to it as the likelihood function $\mathcal{L}(\lambda) = p(d|\lambda)$ of a source. When calculated in full with data and a waveform model, the full likelihood function expresses the probability of a specific waveform model with parameters lambda in the data d. Once we have a likelihood function, we may use a uniform prior or any informative prior to find a posterior probability using the Bayes theorem as given in Eq. (1),

$$p(\lambda|d) \propto p(d|\lambda)p(\lambda). \tag{1}$$

This posterior probability will constrain the properties of each binary, such as mass, spin, and eccentricity. We may infer those parameters using rapid parameter inference on gravitational wave sources via iterative fitting (RIFT): an open source code for parameter estimation (PE) of the binary sources [56]. The above discussion describes the exact likelihood. However, as discussed in Sec. III A, following previous work [57], we will employ a synthetic likelihood model instead of performing an end-to-end parameter inference calculation.

B. Bayesian inference

Now, with the PE of individual sources, we follow the Bayesian framework for population inference. The likelihood of a population parameter Λ is equivalent to the probability of the individual sources given the population parameter Λ is written as follows:

$$\mathcal{L}(\Lambda) \equiv p(d_1, d_2, d_3, \ldots, d_N|\Lambda). \tag{2}$$

Then, using the likelihood in Eq. (2), one can find the posterior probability of Λ as follows:

$$p(\Lambda|d_1, d_2, \ldots, d_N) = \frac{p(\Lambda)p(d_1, d_2, \ldots, d_N|\Lambda)}{p(d_1, d_2, \ldots, d_N)}, \tag{3}$$

where $p(\Lambda|d_1, d_2, d_3, \ldots, d_N)$ is posterior, $p(\Lambda)$ is prior, and $p(d_1, d_2, d_3, \ldots, d_N)$ is normalization constant, also known as evidence.

Considering the generic Bayesian framework above, we conduct our mass and eccentricity distribution analysis. We will use the inhomogeneous Poisson process [58,59] scaled by rate $\mathcal{R} = \frac{dN}{dtdV_c}$ and parametrize by Λ to find the likelihood $\mathcal{L}(\mathcal{R}, \Lambda) \equiv p(D|\mathcal{R}, \Lambda)$ of an astrophysical population given the merger rate and parameter Λ:

$$\mathcal{L}(\mathcal{R}, \Lambda) \propto e^{-\mu(\mathcal{R},\Lambda)} \prod_{n=1}^{N} \int d\lambda \ell_n(\lambda)\mathcal{R}p(\lambda|\Lambda), \tag{4}$$

where $\mu(\mathcal{R}, \Lambda)$ given in Eq. (7) is the expected number of detections under the given population parametrization Λ with the overall rate $\mathcal{R}$. $\ell_n(\lambda) = p(d_n|\lambda)$ is the likelihood of the data d_n given binary parameter. Finally, we will get our posterior as follows:

$$p(\mathcal{R}, \Lambda|D) \propto p(\mathcal{R}, \Lambda)\mathcal{L}(\mathcal{R}, \Lambda) \tag{5}$$

by choosing an appropriate prior $p(\mathcal{R}, \Lambda)$.

These calculations are analytically intractable and must be performed numerically. Specifically, we will use Goodman and Weare's affine invariant Markov chain Monte Carlo (MCMC) [60] to find the posterior distribution of population parameters. This method draws samples from the targeted distribution for Λ, in our case, its eccentric power law model given in Eq. (8), then compares it with the given data (collection of individual events) and stores the best-fit sample. We may iterate this as we need and store multiple sample values until they converge. Our specific implementation is a Python package called EMCEE [61]. We use a low-dimensional model; chains converge to a common region after a few hundred steps. Therefore, we performed our analysis with 100 walkers up to 5000 samples and burned the initial 2500 steps at the plotting stage.

C. Volume time (VT) estimation

To make our study realistic, we include the sensitivity of the LVK instruments. This sensitivity is defined by time volume to which a census of gravitational wave events is sensitive, inferring the product VT. In this expression, V is the characteristic volume with units Gpc^3, which refers to the possible detection region in the sky for the LVK [62], and T is the time duration of making observations at this sensitivity. In practice, VT reflects a suitable time-averaged or cumulative sensitivity, as the true network and sensitivity vary over time.

Existing LVK instruments' sensitivity depends primarily on the mass and, to a lesser extent, on binary spin and (if present) modest eccentricity. Since we neglect spin in this work, we assume the network will have the same VT versus mass as was previously estimated [40] for nonspinning, noneccentric, and nonprecessing binaries. Hence, we briefly explain the calculations; see [40] for details. Equation (6) calculates the orientation averaged sensitive volume [63,64]

$$V(\lambda) = \int P((< D(z))/D_h(\lambda)) \frac{dV_c}{dz} \frac{dz}{1+z}, \tag{6}$$

where $D(z)$ is the luminosity distance for redshift z, D_h is the horizon distance to which source can be seen, and V_c is the comoving volume (for details see [40]). Finally, to compute the average number of detections, we used Eq. (7):

$$\mu(\mathcal{R}, \Lambda) = \int (VT)\lambda\mathcal{R}p(\lambda|\Lambda)d\lambda, \tag{7}$$

where $p(\lambda|\Lambda)$ is the probability density function for a random binary in the Universe to have parameter λ. Keep in mind that λ is equal to all intrinsic and extrinsic parameters.

D. Eccentric power law

Because of gravitational radiation, binary orbital eccentricity decays over time [2]. To unambiguously specify the interpretation of eccentricity, for simplicity, we assume the eccentricity is specified at a reference gravitational wave frequency $f_0 = 10$ Hz, consistent with prior work [52].

There are various weak and pure phenomenological population models proposed in previous studies [55,65,66]. We need a more well-understood theory encompassing all possible formation channels to choose any specific model. Therefore, our analysis used the pure truncated power law defined in [65,66] and modified it to include one-sided Gaussian eccentricity. This model computes the intrinsic probability of m_1, m_2, and ϵ. For simplicity, to focus on binaries with some degree of premerger signal, not necessarily to encompass all astrophysical population models or even rare extreme detections, we kept total mass $M_{\max} = m_1 + m_2 = 100M_\odot$. We also assume that nonzero probability density only exists for $m_{\min} \leq m_2 \leq m_1 \leq m_{\max}$. The generalized form of the truncated power-law model with parameters $\Lambda \equiv (\alpha, \mathcal{R}, k_m, m_{\min}, m_{\max}, \sigma_\epsilon, M_{\max})$ and random variable m_1, m_2, and ϵ has the functional form in Eq. (8) within the provided mass limit,

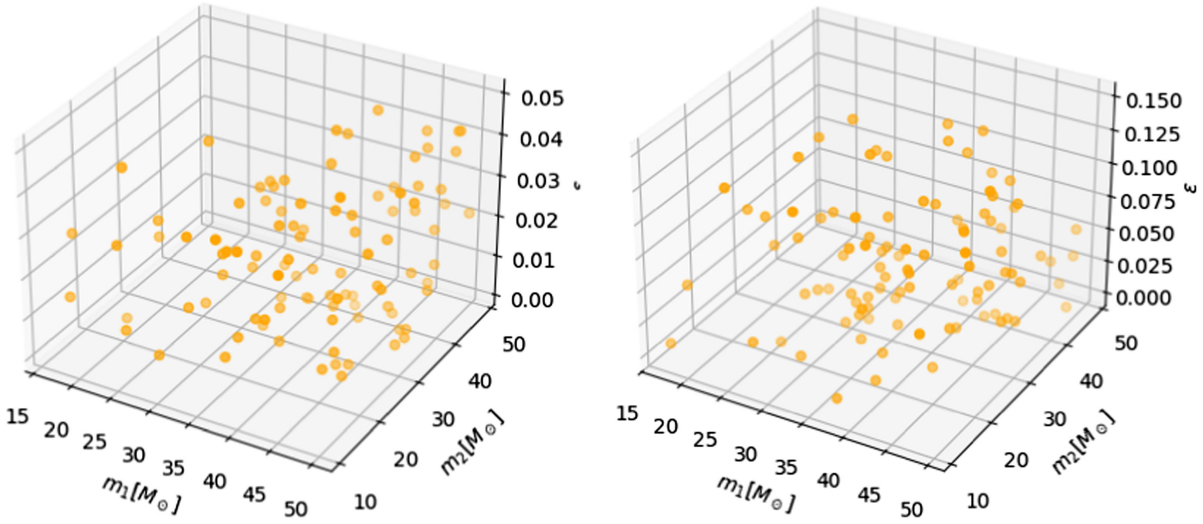

FIG. 1. Synthetic population of EBBH: the lhs shows with $\sigma_\epsilon = 0.05$, the rhs shows with $\sigma_\epsilon = 0.15$.

$$p(m_1, m_2, \epsilon) = C(\alpha, k_m, m_{\min}, m_{\max}, M_{\max}, \epsilon) \times \sqrt{\frac{2}{\pi}} \frac{(m_2/m_1)^{k_m} m_1^{-\alpha} e^{-(\epsilon/\sqrt{2}\sigma_\epsilon)^2}}{(m_1 - m_{\min})\sigma_\epsilon}, \quad (8)$$

where α is the power law index, $\mathcal{R}$ is the merger rate, $m_{\min}$, $m_{\max}$ are the minimum and maximum masses of the binary components in the population, and σ_ϵ is the orbital eccentricity distribution. Equation (8) represents a truncated power law for primary mass m_1 with index $-\alpha$ and conditional power law distribution $p(m_2|m_1)$ for secondary mass m_2 using power law, and one-sided Gaussian distribution for orbital eccentricity ϵ. For our analysis, we defined a constant of integration equal to $\int_V dm_1 dm_2 d\epsilon p(m_1, m_2, \epsilon) = 1$. Our detectors are sensitive to high-mass BBHs. Therefore, we will use $k_m = 0$ throughout the studies. As a result, we have our reduced form of the truncated power law in Eq. (9):

$$p(m_1, m_2, \epsilon) = \sqrt{\frac{2}{\pi}} \frac{m_1^{-\alpha} e^{-(\epsilon/\sqrt{2}\sigma_\epsilon)^2}}{(m_1 - m_{\min})\sigma_\epsilon}. \quad (9)$$

III. SYNTHETIC POPULATION

We have generated two synthetic populations with conservative case $\sigma_\epsilon = 0.05$ and optimistic case $\sigma_\epsilon = 0.15$ by choosing the power law parameters $\alpha = -1$, $m_{\min} = 10$, and $m_{\max} = 50$. Starting with 10000 synthetic sources for each population, we find the probability for each event to be detected by computing the VT of each source. Finally, we weighed based on these VTs and randomly picked $N = 100$ sources from each population to perform our analysis. To be concrete, to eliminate the impact of Poisson counting statistics on our event rate inference, and guarantee that both synthetic populations should favor the same event rate, we have specifically adopted a known event count for each population (i.e., $N = 100$). As a result, the implied observing time ($T = 248$d) guarantees the expected event count will be exactly $\mu = 100$ for the true population parameters for each synthetic population. Our analysis assumed the fixed rate density per comoving volume and no evolution. Our injected populations with $\sigma_\epsilon = 0.05$ and $\sigma_\epsilon = 0.15$ are shown in Fig. 1.

A. Eccentric synthetic population

To make our study more realistic, we must add the measurement error in each source. Rather than generate synthetic gravitational wave sources and perform full Bayesian inference, following previous work [57] we generate mock measurement errors motivated by real parameter inference investigations. Hence, chirp mass and symmetric mass ratio are well constrained compared to the primary and secondary masses of BBH. We compute them for each event in a population by using the following relation:

$$M_{ecc}^T = \frac{(m_1 m_2)^{3/5}}{(m_1 + m_2)^{1/5}}, \quad (10)$$

$$\eta_{ecc}^T = \frac{(m_1 m_2)}{(m_1 + m_2)^2}, \quad (11)$$

where M_{ecc}^T, η_{ecc}^T, m_1, and m_2 are the true chirp mass, symmetric mass ratio, primary mass, and secondary mass of an eccentric binary, respectively. Furthermore, using the following relations, we add the measurement errors in the M_{ecc}^T and η_{ecc}^T:

$$M_{ecc} = M_{ecc}^T \left(1 + \beta(r_0 + r)\frac{12}{\rho}\right), \quad (12)$$

$$\eta_{ecc} = \eta_{ecc}^T \left(1 + 0.03(r_0' + r')\frac{12}{\rho}\right). \quad (13)$$

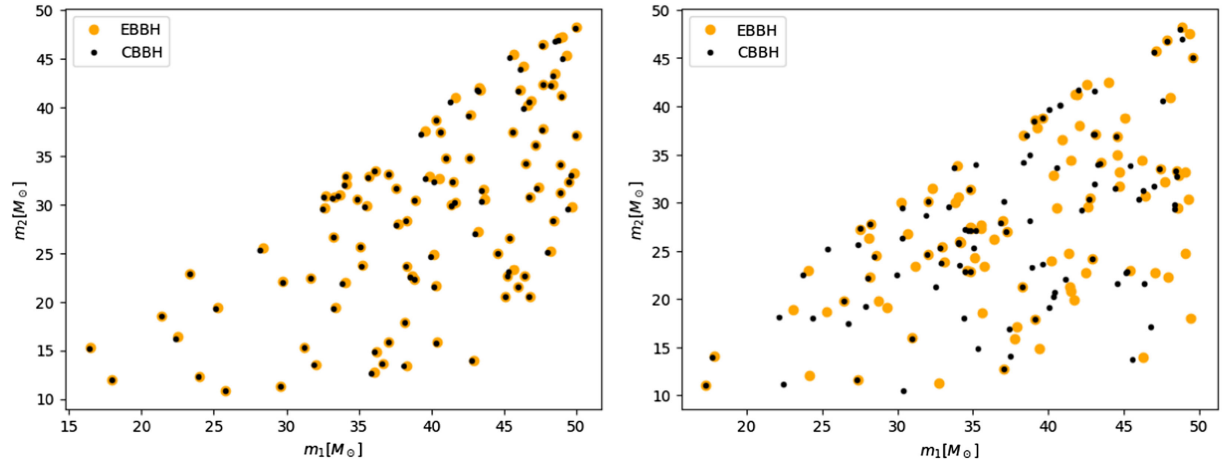

FIG. 2. Mass shift after removing eccentricity: the lhs shows with $\sigma_\epsilon = 0.05$, the rhs shows with $\sigma_\epsilon = 0.15$.

Here r_0 and r_0' are the random numbers drawn from the standard normal distribution, which will shift the mean of the M_{ecc} and η_{ecc} distribution with respect to M_{ecc}^T and η_{ecc}^T. The r and r' are the independent and identically distributed arrays of those randomly generated numbers to spread the distribution. The measurement uncertainty is inversely proportional to signal-to-noise ratio ρ, drawn from the distribution $p(\rho) \propto \rho^{-4}$, which holds for isotropically distributed sources in a static Universe, subject to the threshold $\rho \geq 8$ for detection. Following Sec. III D of [67], we estimate $\beta \simeq 0.5(v/0.2)^7/w$, where v is an estimated post-Newtonian orbital velocity at a reference frequency of 20 Hz, $w = \rho/12$, and ρ is drawn from a Euclidean SNR distribution $P(> \rho) \propto 1/\rho^3$.

Finally, after adding the measurement errors in the M_{ecc}^T and η_{ecc}, we will convert them back to m_1 and m_2 to perform our analysis. We used the following relation for conversion, and it will provide the masses based on the condition $m_1 \geq m_2$:

$$m_1 = \frac{1}{2} M_{ecc} \eta_{ecc}^{-3/5} (1 + \sqrt{\eta_v}), \tag{14}$$

$$m_2 = \frac{1}{2} M_{ecc} \eta_{ecc}^{-3/5} (1 - \sqrt{\eta_v}), \tag{15}$$

where $\eta_v = 1\text{–}4\eta_{ecc}$, we kept the samples with non-negative values and ignored the negative samples to avoid the square root issues.

We also added the absolute error in the eccentricity distribution using the truncated normal distribution (to keep ϵ positive) scaling at 0.06 and 0.2 for modest and optimistic eccentricity cases, respectively. For our study, we have the flexibility to make arbitrary choices in the distribution parameters, a feature that underscores the adaptability of our methodology.

To summarize, following previous work, our semianalytic per-event likelihood model is a simple (truncated) Gaussian approximation in suitable coordinates, with shape and structure motivated by the leading-order phase and likelihood expected from inspiral-dominated sources. While this approximation's scale and correlations will not mimic realistic posteriors for the most massive sources, whose gravitational-wave signal is merger dominated, this estimate nonetheless has qualitatively correct behavior at the highest masses (i.e., broad posteriors) and, consistent with prior work, is sufficient for our proof-of-concept study.

B. Circular synthetic population

To compare the synthetic EBBH population with the CBBH, we estimate how our sources would be characterized by parameter inference that omitted the effects of eccentricity:

$$M_{\rm ecc} = \frac{M_{\rm cir}}{\left(1 - \frac{157}{24}\epsilon^2\right)^{3/5}}. \tag{16}$$

Our ansatz for source identification and characterization is that the best-fitting parameters and posteriors are directly related to the true posteriors, except that the recovered chirp mass is given by Eq. (16). Therefore, we take the posterior of each event of eccentric synthetic populations generated in Sec. III A and applied the scaling using Eq. (16) on primary and secondary masses to remove the eccentricity [52]. As a result, we have the CBBH population with the same number of events and same posterior size as the EBBH population.

The significant effect of scaling is the mass shift, which can be observed in Fig. 2. In that figure, the left-hand side shows the mass shift of the first population generated with a lower $\sigma_\epsilon = 0.05$, which leads to a lesser mass shift. However, the right hand side of Fig. 2 shows the significant mass shift after removing the eccentric component due to the optimistic case of eccentricity distribution.

IV. POPULATION INFERENCE OF EBBH AND CBBH

We have generated two populations using conservative $\sigma_\epsilon = 0.05$ and optimistic $\sigma_\epsilon = 0.15$ to show the effect of

TABLE I. Injected parameters to generate synthetic population and priors used for Bayesian inference.

Quantity	$\log_{10}\left(\frac{\mathcal{R}}{\mathrm{Gpc}^{-3}\ \mathrm{yr}^{-1}}\right)$	α	$m_{\min}[M_\odot]$	$m_{\max}[M_\odot]$	σ_ϵ
Synthetic population	2	-1	10	50	$\{0.05, 0.15\}$
Prior range	$[-5, 5]$	$[-5, 5]$	[1–20]	[30–100]	[0–0.5]
Prior distribution	Log uniform	Uniform	Uniform	Uniform	Uniform

eccentricity on the masses. We made the inference on both populations using Bayesian inference with uniform priors given in Table I, and we used a likelihood given in Eq. (2). We estimated posterior distribution by collecting ample samples using the MCMC method. The contour plots of the posterior distribution for recovered parameters are given in Figs. 3 and 4, which show the results of population inference under the most conservative and optimistic case.

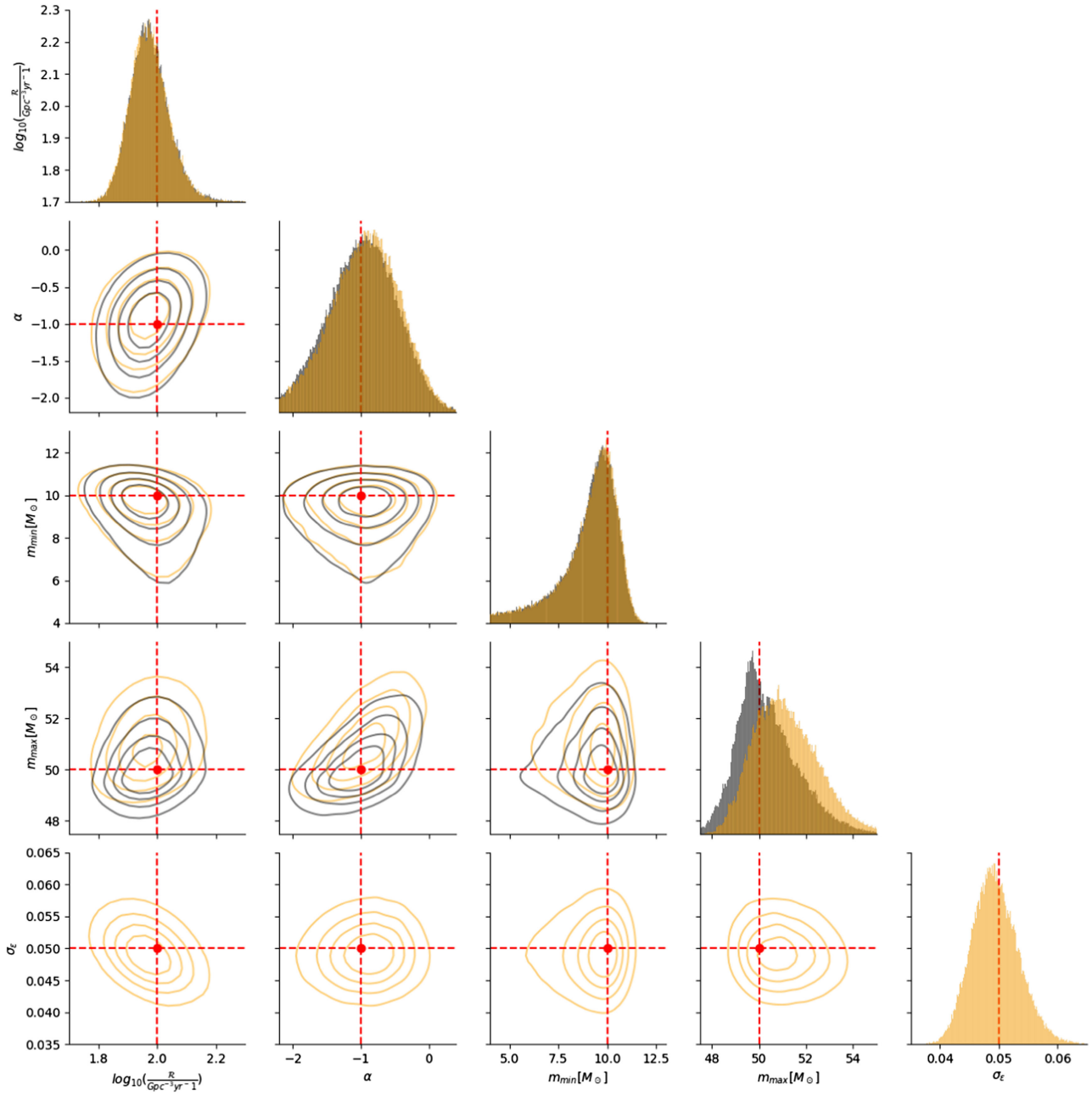

FIG. 3. Corner plots of EBBH (orange) and CBBH (black) for $\sigma_\epsilon = 0.05$.

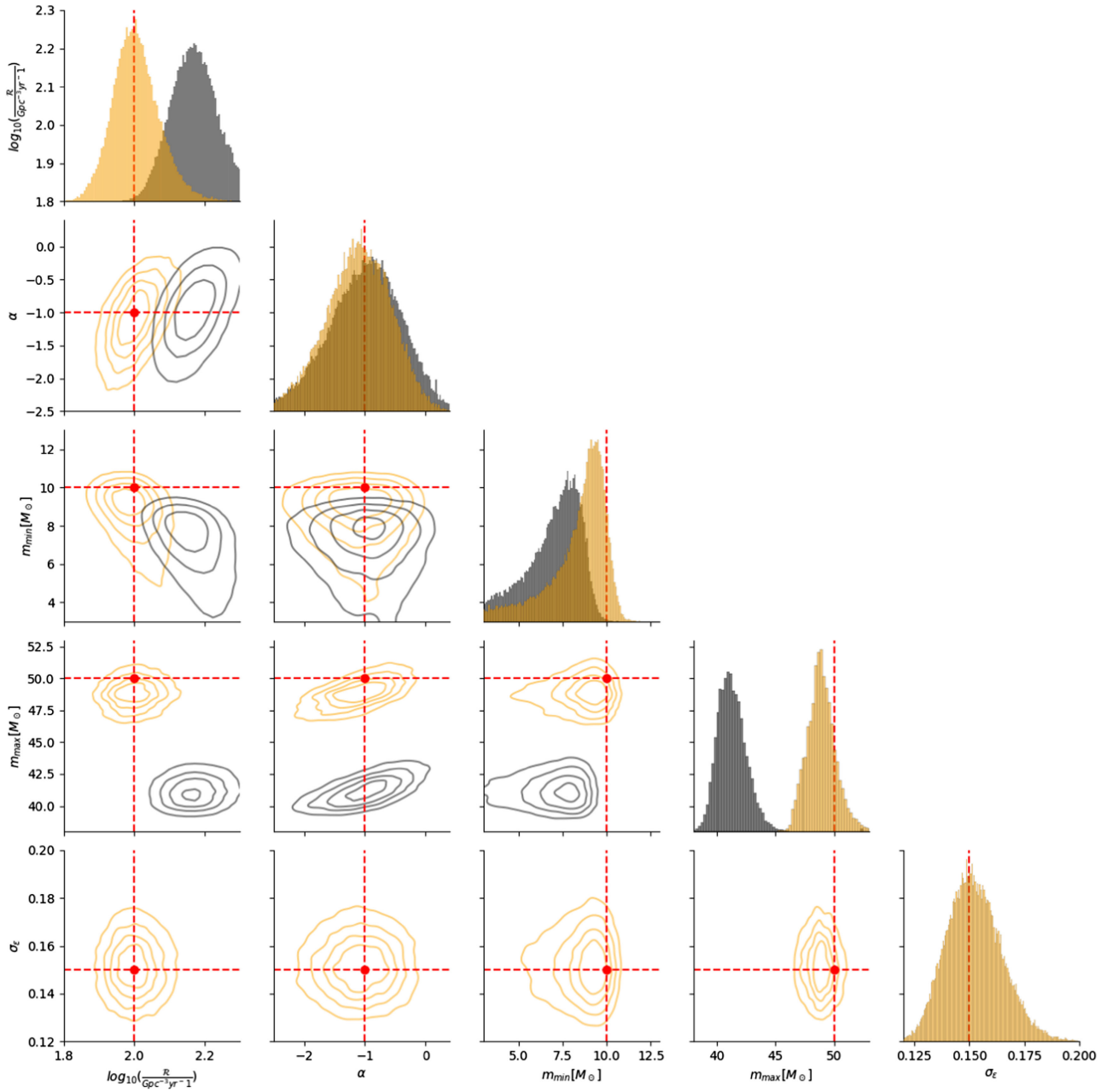

FIG. 4. Corner plots of EBBH (orange) and CBBH (black) for $\sigma_\epsilon = 0.15$.

In those figures, the black color shows the results of CBBH, the orange color shows the results of EBBH, and the red color shows the true injected values.

Figure 3 shows that in the limit of extremely small eccentricity, the impact of eccentricity is minimal on population constraints. This result depends, of course, on our assumption that all binaries are equally likely to have eccentricity and that our measurement uncertainty in eccentricity is both independent of mass and reasonably small, both optimistic assumptions. Most notable is the impact of neglecting eccentricity for higher eccentric binaries. If the eccentricity is neglected, then the population inference is biased away from true values: the black contours in Fig. 4 do not include the true values for the injected population. This bias is expected, as the eccentricity is a significant parameter in the population model, particularly at the higher eccentricities.

In addition, we also performed our analysis to check the minimum number of eccentric events to recover the injected $\sigma_\epsilon = 0.05$, each with a measurement error of 0.06. Our results show that we can recover the distribution of σ_ϵ even with five eccentric events. The increment in the number of events leads towards narrower posterior distribution of eccentricity distribution. So, the more eccentric

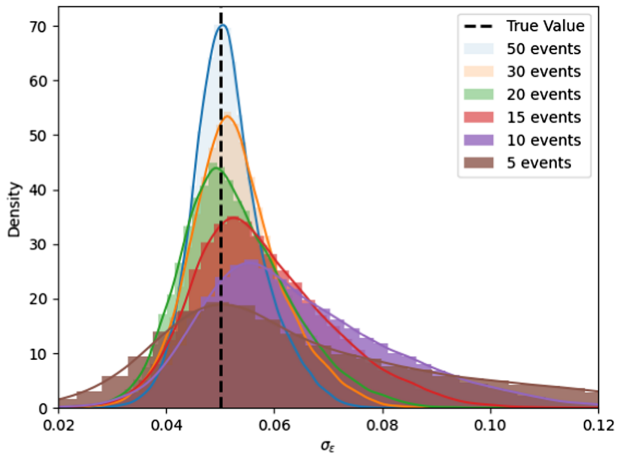

FIG. 5. Histogram for eccentricity distribution with different numbers of events.

events, the better the recovered value of σ_ϵ. As we can recover the mass and eccentricity distribution with a small number of events, it is equally essential to have a large number of events to get a more accurate recovery of rate and model parameter α. The pattern of recovered eccentricity distribution from broader to narrow is evident in Fig. 5 with different numbers of events.

V. DISCUSSION

The sensitivity of LVK detectors is increasing with time, leading to more detection in each observing run. We will have hundreds of events in future runs, and with the ongoing O4 run, detections could occur as frequently as every other day [68,69]. Interestingly, the new detections lead us to reasonable disagreement on the masses, spin, event rate, and formation scenarios [70,71], which pushes researchers to develop new models [72,73], to provide more information about the observable GW [74–76]. Therefore, identifying and understanding the populations of EBBH with a growing number of detections will give us more insightful information about the formation and evolution of massive stars from birth to death over cosmic time.

Until now, all of the confirmed detections are consistent with nearly circular orbits, and there can be various reasons for this bias. The first potential reason for getting circular orbits is that eccentric effects are more evident in low-mass events, and current searches are more efficient for higher-mass mergers. Second, it may result from selection biases in the waveforms because LVK detectors only use circular waveforms for parameter estimation (PE), which better present binaries evolved in an isolated environment than the dynamically evolved ones.

Studies show that we must consider the multiple formation channels to understand the population better because a single channel may not contribute more than 70% of the observation sample of BBH [77]. In addition, we may have stellar mass higher eccentric mergers at the lower frequency searches [78,79], which can be measurable by detectors like Laser Interferometer Space Antenna (LISA) [80]. These observations would allow for long-term tracking of BBH orbital properties, which can be used to infer the formation mechanism better [81]. So, it is critical for astrophysical implications to assess eccentricity distribution to infer their formation better.

VI. CONCLUSION

In this work, we demonstrate how one can recover the effects of eccentricity in a binary black hole population using a parametric model. Specifically, we extended a simple power law model to include a one-sided Gaussian eccentricity distribution for BBH. We verified that our approach can recover the properties of two specific injected populations, generating a large synthetic population with known values $\log_{10}(\mathcal{R}) = 2$, $\alpha = -1$, $m_{\rm min} = 10M_\odot$, $m_{\rm max} = 50M_\odot$, and $\sigma_\epsilon = 0.05, 0.15$.

We then demonstrated that analyses using fewer events could identify the signatures of eccentricity. However, longer signals may be needed to distinguish the eccentricity from the spin precession [82]. We expect ∼1% to ∼17% mass shift for the modest ($\sigma_\epsilon = 0.05$) to the optimistic ($\sigma_\epsilon = 0.15$) case, respectively, based on Eq. (16). We observed a 12.5% difference in our population parameters recovery between EBBH and CBBH. Finally, we demonstrated that the neglect of eccentricity can bias the recovered population parameters if the eccentricity in the population is frequently large, evident in Table II.

For this analysis, we restricted our inference only to BBH, but in the future, we aim to include eccentricity in other binary models, such as BNS and NSBH models. We also plan to modify the high-dimensional population models [40] to add eccentricity, spin, and precessing BBH.

TABLE II. Parameter constraints: EBBH vs CBBH for $\sigma_\epsilon = 0.15$.

Inference	$\log_{10}\left(\frac{\mathcal{R}}{\mathrm{Gpc^{-3}\,yr^{-1}}}\right)$	α	$m_{\rm min}[M_\odot]$	$m_{\rm max}[M_\odot]$	σ_ϵ
EBBH	$2.02^{+0.07}_{-0.07}$	$-0.26^{+0.41}_{-0.45}$	$9.03^{+1.13}_{-2.06}$	$52.93^{+1.93}_{-1.78}$	$0.16^{+0.01}_{-0.01}$
CBBH	$2.24^{+0.10}_{-0.08}$	$-0.02^{+0.41}_{-0.47}$	$6.56^{+1.54}_{-2.32}$	$43.79^{+1.50}_{-1.34}$	⋯

ACKNOWLEDGMENTS

The authors acknowledge the computational resources provided by the LIGO Laboratory's CIT cluster, which is supported by National Science Foundation Grants No. PHY-0757058 and No. PHY0823459.

[1] V. P. Frolov and A. Zelnikov, *Introduction to Black Hole Physics* (Oxford University Press, New York, 2011), ISBN 9780199692293.
[2] P. C. Peters and J. Mathews, Phys. Rev. **131**, 435 (1963).
[3] J. Aasi, B. P. Abbott, R. Abbott, T. Abbott *et al.*, Classical Quantum Gravity **32**, 074001 (2015).
[4] T. Accadia, F. Acernese, M. Alshourbagy, P. Amico *et al.*, J. Instrum. **7**, P03012 (2012).
[5] F. Acernese, M. Agathos, K. Agatsuma, D. Aisa *et al.*, Classical Quantum Gravity **32**, 024001 (2015).
[6] T. Akutsu, M. Ando, K. Arai, Y. Arai, S. Araki, A. Araya, N. Aritomi, Y. Aso, S. Bae, Y. Bae *et al.*, Prog. Theor. Exp. Phys. **2021**, 05A101 (2021).
[7] B. P. Abbott, R. Abbott, T. D. Abbott, S. Abraham, F. Acernese, K. Ackley, C. Adams, R. X. Adhikari, V. B. Adya, C. Affeldt *et al.*, Phys. Rev. X **9**, 031040 (2019).
[8] R. Abbott, T. D. Abbott, S. Abraham, F. Acernese, K. Ackley, A. Adams, C. Adams, R. X. Adhikari, V. B. Adya, C. Affeldt *et al.*, Phys. Rev. X **11**, 021053 (2021).
[9] R. Abbott, T. D. Abbott, F. Acernese, K. Ackley, C. Adams, N. Adhikari, R. X. Adhikari, V. B. Adya *et al.* (LIGO Scientific and Virgo Collaborations), Phys. Rev. D **109**, 022001 (2024).
[10] R. Abbott, T. D. Abbott, F. Acernese, K. Ackley, C. Adams, N. Adhikari, R. X. Adhikari, V. B. Adya, C. Affeldt, D. Agarwal *et al.*, Phys. Rev. X **13**, 041039 (2023).
[11] I. Mandel and A. Farmer, Phys. Rep. **955**, 1 (2022).
[12] M. Mapelli, Front. Astron. Space Sci. **7** (2020).
[13] N. Steinle and M. Kesden, Phys. Rev. D **103**, 063032 (2021).
[14] F. Antonini, S. Chatterjee, C. L. Rodriguez, M. Morscher, B. Pattabiraman, V. Kalogera, and F. A. Rasio, Astrophys. J. **816**, 65 (2016).
[15] F. Antonini, M. Gieles, and A. Gualandris, Mon. Not. R. Astron. Soc. **486**, 5008 (2019).
[16] P. C. Peters, Phys. Rev. **136**, B1224 (1964).
[17] C. L. Rodriguez, P. Amaro-Seoane, S. Chatterjee, K. Kremer, F. A. Rasio, J. Samsing, C. S. Ye, and M. Zevin, Phys. Rev. D **98**, 123005 (2018).
[18] M. Zevin, J. Samsing, C. Rodriguez, C.-J. Haster, and E. Ramirez-Ruiz, Astrophys. J. **871**, 91 (2019).
[19] J. Samsing, Phys. Rev. D **97**, 103014 (2018).
[20] C. L. Rodriguez, P. Amaro-Seoane, S. Chatterjee, and F. A. Rasio, Phys. Rev. Lett. **120**, 151101 (2018).
[21] F. Antonini, N. Murray, and S. Mikkola, Astrophys. J. **781**, 45 (2014).
[22] I. Romero-Shaw, P. D. Lasky, and E. Thrane, Astrophys. J. **940**, 171 (2022).
[23] H. L. Iglesias, J. Lange, I. Bartos, S. Bhaumik, R. Gamba, V. Gayathri, A. Jan, R. Nowicki, R. O'Shaughnessy, D. Shoemaker *et al.*, Astrophys. J. **972**, 65 (2024).
[24] R. Gamba, M. Breschi, G. Carullo, S. Albanesi, P. Rettegno, S. Bernuzzi, and A. Nagar, Nat. Astron. **7**, 11 (2022).
[25] Y. Xu and E. Hamilton, Phys. Rev. D **107**, 103049 (2023).
[26] R. Gamba, M. Breschi, G. Carullo, S. Albanesi, P. Rettegno, S. Bernuzzi, and A. Nagar, Nat. Astron. **7**, 11 (2023).
[27] V. Gayathri, J. Healy, J. Lange, B. O'Brien, M. Szczepanczyk, I. Bartos, M. Campanelli, S. Klimenko, C. Lousto, and R. O'Shaughnessy, Nat. Astron. **6**, 344 (2022).
[28] I. Romero-Shaw, P. D. Lasky, E. Thrane, and J. Calderón Bustillo, Astrophys. J. Lett. **903**, L5 (2020).
[29] H. L. Iglesias, J. Lange, I. Bartos, S. Bhaumik, R. Gamba, V. Gayathri, A. Jan, R. Nowicki, R. O'Shaughnessy, D. Shoemaker *et al.*, arXiv:2208.01766.
[30] A. Ramos-Buades, A. Buonanno, and J. Gair, Phys. Rev. D **108**, 124063 (2023).
[31] E. Huerta, P. Kumar, S. T. McWilliams, R. O'Shaughnessy, and N. Yunes, Phys. Rev. D **90**, 084016 (2014).
[32] R. Gold and B. Brügmann, Phys. Rev. D **88**, 064051 (2013).
[33] I. Hinder, F. Herrmann, P. Laguna, and D. Shoemaker, Phys. Rev. D **82**, 024033 (2010).
[34] J. Healy and C. O. Lousto, Phys. Rev. D **105**, 124010 (2022).
[35] A. Nagar, J. Healy, C. O. Lousto, S. Bernuzzi, and A. Albertini, Phys. Rev. D **105**, 124061 (2022).
[36] M. Campanelli, C. O. Lousto, H. Nakano, and Y. Zlochower, Phys. Rev. D **79**, 084010 (2009).
[37] M. E. Lower, E. Thrane, P. D. Lasky, and R. Smith, Phys. Rev. D **98**, 083028 (2018).
[38] X. Fang, T. A. Thompson, and C. M. Hirata, Astrophys. J. **875**, 75 (2019).
[39] S. Wu, Z. Cao, and Z.-H. Zhu, Mon. Not. R. Astron. Soc. **495**, 466 (2020).
[40] D. Wysocki, J. Lange, and R. O'Shaughnessy, Phys. Rev. D **100** (2019).
[41] M. Dominik, E. Berti, R. O'Shaughnessy, I. Mandel, K. Belczynski, C. Fryer, D. E. Holz, T. Bulik, and F. Pannarale, Astrophys. J. **806**, 263 (2015).
[42] J. Samsing, A. S. Hamers, and J. G. Tyles, Phys. Rev. D **100**, 043010 (2019).
[43] K. Belczynski, A. Heger, W. Gladysz, A. J. Ruiter, S. Woosley, G. Wiktorowicz, H.-Y. Chen, T. Bulik, R. O'Shaughnessy, D. E. Holz *et al.*, Astron. Astrophys. **594**, A97 (2016).
[44] C. Talbot and E. Thrane, Phys. Rev. D **96**, 023012 (2017).
[45] A. Miyamoto, T. Kinugawa, T. Nakamura, and N. Kanda, Phys. Rev. D **96**, 064025 (2017).

[46] W. M. Farr, S. Stevenson, M. C. Miller, I. Mandel, B. Farr, and A. Vecchio, Nature (London) **548**, 426 (2017).
[47] R. O'Shaughnessy, D. Gerosa, and D. Wysocki, Phys. Rev. Lett. **119**, 011101 (2017).
[48] D. Wysocki, D. Gerosa, R. O'Shaughnessy, K. Belczynski, W. Gladysz, E. Berti, M. Kesden, and D. E. Holz, Phys. Rev. D **97**, 043014 (2018).
[49] B. P. Abbott, R. Abbott, T. D. Abbott, S. Abraham *et al.*, Astrophys. J. **882**, L24 (2019).
[50] M. Zevin, I. M. Romero-Shaw, K. Kremer, E. Thrane, and P. D. Lasky, Astrophys. J. Lett. **921**, L43 (2021).
[51] K. J. Wagner and R. O'Shaughnessy, arXiv:2402.08039.
[52] M. Favata, C. Kim, K. G. Arun, J. Kim, and H. W. Lee, Phys. Rev. D **105**, 023003 (2022).
[53] B. Sun, Z. Cao, Y. Wang, and H.-C. Yeh, Phys. Rev. D **92**, 044034 (2015).
[54] M. Fishbach and D. E. Holz, Astrophys. J. **851**, L25 (2017).
[55] C. Talbot and E. Thrane, Astrophys. J. **856**, 173 (2018).
[56] J. Lange, R. O'Shaughnessy, and M. Rizzo, arXiv:1805.10457.
[57] I. Mandel, W. M. Farr, A. Colonna, S. Stevenson, P. Tiňo, and J. Veitch, Mon. Not. R. Astron. Soc. **465**, 3254 (2017).
[58] I. Mandel, W. M. Farr, and J. R. Gair, Mon. Not. R. Astron. Soc. **486**, 1086 (2019).
[59] T. J. Loredo, AIP Conf. Proc. **735**, 195 (2004).
[60] J. Goodman and J. Weare, Commun. Appl. Math. Comput. Sci. **5**, 65 (2010).
[61] D. Foreman-Mackey, D. W. Hogg, D. Lang, and J. Goodman, Publ. Astron. Soc. Pac. **125**, 306 (2013).
[62] L. S. Finn and D. F. Chernoff, Phys. Rev. D **47**, 2198 (1993).
[63] B. P. Abbott, R. Abbott, T. D. Abbott, M. R. Abernathy *et al.*, Astrophys. J. **818**, L22 (2016).
[64] R. O'Shaughnessy, V. Kalogera, and K. Belczynski, Astrophys. J. **716**, 615 (2010).
[65] B. Abbott, R. Abbott, T. Abbott, M. Abernathy *et al.*, Phys. Rev. X **6**, 041015 (2016).
[66] M. Fishbach and D. E. Holz, Astrophys. J. **851**, L25 (2017).
[67] J. Wofford, A. Yelikar, H. Gallagher, E. Champion, D. Wysocki, V. Delfavero, J. Lange, C. Rose, V. Valsan, S. Morisaki *et al.*, Phys. Rev. D **107**, 024040 (2023).
[68] B. Abbott, R. Abbott, T. Abbott, M. Abernathy *et al.*, Phys. Rev. X **6**, 041015 (2016).
[69] B. P. Abbott, R. Abbott, T. D. Abbott, M. R. Abernathy *et al.*, Astrophys. J. **833**, L1 (2016).
[70] B. Abbott, R. Abbott, T. Abbott, M. Abernathy *et al.*, Phys. Rev. X **6**, 041015 (2016).
[71] B. P. Abbott, R. Abbott, T. D. Abbott, M. R. Abernathy *et al.*, Astrophys. J. **818**, L22 (2016).
[72] I. Mandel and S. E. de Mink, Mon. Not. R. Astron. Soc. **458**, 2634 (2016).
[73] P. Marchant, N. Langer, P. Podsiadlowski, T. M. Tauris, and T. J. Moriya, Astron. Astrophys. **588**, A50 (2016).
[74] E. Barausse, R. Brito, V. Cardoso, I. Dvorkin, and P. Pani, Classical Quantum Gravity **35**, 20LT01 (2018).
[75] B. Abbott, R. Abbott, T. Abbott, M. Abernathy *et al.*, Phys. Rev. Lett. **116**, 131102 (2016).
[76] I. Dvorkin, E. Vangioni, J. Silk, J.-P. Uzan, and K. A. Olive, Mon. Not. R. Astron. Soc. **461**, 3877 (2016).
[77] M. Zevin, S. S. Bavera, C. P. L. Berry, V. Kalogera, T. Fragos, P. Marchant, C. L. Rodriguez, F. Antonini, D. E. Holz, and C. Pankow, Astrophys. J. **910**, 152 (2021).
[78] A. Sesana, Phys. Rev. Lett. **116**, 231102 (2016).
[79] X. Chen and P. Amaro-Seoane, Astrophys. J. **842**, L2 (2017).
[80] LISA Pathfinder Collaboration, J. Phys. Conf. Ser. **840**, 012001 (2017).
[81] K. Breivik, C. L. Rodriguez, S. L. Larson, V. Kalogera, and F. A. Rasio, Astrophys. J. **830**, L18 (2016).
[82] I. M. Romero-Shaw, D. Gerosa, and N. Loutrel, Mon. Not. R. Astron. Soc. **519**, 5352 (2023).